RSC Advances

PAPER

View Article Online
View Journal | View Issue

Cite this: *RSC Adv.*, 2023, **13**, 14306

Pronounced effect of yttrium oxide on the activity of Pd/rGO electrocatalyst for formic acid oxidation reaction†

Muhammad Sofian,[a] Fatima Nasim,[a] Hassan Ali*[a] and Muhammad Arif Nadeem *[ab]

A highly efficient and stable electrocatalyst comprised of yttrium oxide (Y_2O_3) and palladium nanoparticles has been synthesized *via* a sodium borohydride reduction approach. The molar ratio of Pd and Y was varied to fabricate various electrocatalysts and the oxidation reaction of formic acid was checked. X-ray photoelectron spectroscopy (XPS), transmission electron microscopy (TEM), and X-ray powder diffraction (XRD) are used to characterize the synthesized catalysts. Among the synthesized catalysts (Pd_yY_x/rGO), the optimized catalyst *i.e.*, Pd_6Y_4/rGO exhibits the highest current density (106 mA cm^{-2}) and lowest onset potential compared to Pd/rGO (28.1 mA cm^{-2}) and benchmark Pd/C (21.7 mA cm^{-2}). The addition of Y_2O_3 to the rGO surface results in electrochemically active sites due to the improved geometric structure and bifunctional components. The electrochemically active surface area 119.4 m^2 g^{-1} is calculated for Pd_6Y_4/rGO, which is ~1.108, ~1.24, ~1.47 and 1.55 times larger than Pd_4Y_6/rGO, Pd_2Y_8/rGO, Pd/C and Pd/rGO, respectively. The redesigned Pd structures on Y_2O_3-promoted rGO give exceptional stability and enhanced resistance to CO poisoning. The outstanding electrocatalytic performance of the Pd_6Y_4/rGO electrocatalyst is ascribed to uniform dispersion of small size palladium nanoparticles which is possibly due to the presence of yttrium oxide.

Received 24th March 2023
Accepted 29th April 2023

DOI: 10.1039/d3ra01929b

rsc.li/rsc-advances

Introduction

Fossil fuels have historically been employed as an energy source since ancient times because of their convenience and effectiveness, but this has resulted in tremendous oil consumption, energy depletion, and environmental degradation.[1,2] Although the extraction and use of fossil fuels have significantly raised the quality of human life, the traditional methods of energy production and consumption are becoming inappropriate for long-term use by humans. Substantial efforts are being made to create cutting-edge energy storage and conversion technologies in order to address the impeding energy crisis and the linked issues of environmental pollution.[3–6] Fuel cells are potential energy conversion technologies that produce electricity from the stored energy in the chemical bonds of fuel. The anode of a direct formic acid fuel cell (DFAFC), converts formic acid to carbon dioxide (CO_2), whereas at the cathode reduction of oxygen take place.[7] Fuel cells using formic acid as direct fuel have received a lot of attention over the past 20 years and are anticipated to be crucial in the advancement of sustainable energy technologies for small, portable and mobile appliances due to the ease of storage, solubility in water at room temperature, low fuel cross over across proton exchange membrane, high energy density, environmental friendliness, and non-flammability.[8–12] Since the 1970s, the formic acid oxidation process (FAOR) has been receiving lot of attention.[13] Formic acid (FA) oxidation often occurring through direct dehydrogenation pathway involves the conversion of FA to CO_2 while the indirect route involves the production of toxic intermediate (CO_{ads}).[14,15]

The indirect process drastically reduces formic acid fuel cell efficiency with potentially toxic intermediates.[16] Highly stable nanomaterials based on platinum (Pt) are capable of catalyzing formic acid oxidation. However, the indirect dehydration process is aided by Pt's susceptibility to CO_{ads} adsorption.[17,18] The commercialization of DFAFC is still hampered by the cost and limited cell activity of the catalysts employed in fuel cells. Palladium (low-cost metal, approximately 1/3 to platinum) and palladium-based nanomaterials, on the other hand, can catalyze formic acid oxidation through the direct route with less susceptibility to CO_{ads}. However, a low catalytic activity and low electrochemical stability of palladium based catalysts hinder their application in fuel cells.[18–21] Therefore, it is crucial to develop Pd nanomaterials with efficient formic acid electrocatalytic activity in order to support the widespread use of DFAFC. Component regulation of electrocatalyst is a useful

[a]*Catalysis and Nanomaterials Lab 27, Department of Chemistry, Quaid-i-Azam University, Islamabad 45320, Pakistan. E-mail: hassanali471@gmail.com; manadeem@qau.edu.pk*

[b]*Pakistan Academy of Sciences, 3-Constitution Avenue Sector G-5/2, Islamabad, Pakistan*

† Electronic supplementary information (ESI) available. See DOI: https://doi.org/10.1039/d3ra01929b

strategy for enhancing the stability and electroactivity of Pd-based nanomaterials.[22] A lot of work has been done to boost the activity of Pd-based electrocatalysts by the formation of alloy, modification of support material and building unique nanostructures.[21,23–25] Bimetallic palladium based nanocatalysts such as PdNi, PdAu, PdGa, PdCu, and PdRu have shown improved activities compared to palladium nanoparticles (Pt/C). The incorporation of another metal enhanced the electrocatalytic capabilities of the material towards formic acid oxidation reaction.[26] Recent studies show that metal oxide compounds can function as promoters and greatly increase the catalytic efficiency of metallic nanocrystals. The shape of the deposited catalytic metal nanoparticles, its dispersion, and electronic level are significantly affected by the promoters used. They can also change the adsorption process and provide the catalyst with anti-poisoning function. Pd–CeO_2/C has shown increased electrocatalytic activity than the standard Pd/C and better kinetics for formic acid oxidation according to Wang and coworkers.[73] Gu *et al.* proposed that oxygen vacancies in CeO_2 operate as active sites to oxidize poisonous species (CO) that have been adsorbed on Pt, resulting in outstanding activity for anodic methanol oxidation over Pt–CeO_2/C catalyst.[27] A novel catalyst (PdPt/CeO_2/C) that show excellent result in the formic acid electrooxidation at anode was introduced by Yang *et al.* (11).[28] Bulut *et al.* employed MnO_2 as promoter in Pd based catalyst and observed the enhancement in electrocatalytic activity towards formic acid oxidation (FAO).[29] likewise, Maturost and co-workers demonstrated improved stability and activity towards FA oxidation by promoting Pd *via* copper.[30] Similarly, Hossain *et. al.* noted improvement in electrocatalytic activity of Pd by using Nickle oxide as promoter towards FA oxidation.[31] Likewise, Feng *et al.* reported that electrocatalytic performance during oxidation of formic acid is enhanced with the incorporation of europium oxide into Pd based catalysts.[32] Electrocatalysts conductivity is enhanced, when carbon nanofibers, mesoporous carbon, and carbon nanotubes *etc.* have been used as support material in electrocatalytic applications. However, the corrosion of carbon based support during the environmental conditions of fuel cells decreases the electrochemical surface area, resulting in performance deterioration.[33] It is challenging to deposit extremely tiny and evenly dispersed metal nanocrystals due to the lack of binding sites on pristine CNT surfaces.[34] The thin microporosity, which makes mass transport operations challenging, and lack of electrical conductivity of activated carbon limit their employment as electrocatalysts.[35] Recently, reduced graphene oxide (rGO) has gained popularity because of huge surface area, tunable functionalities, chemical inertness, ease of availability, porosity, and cost-effectiveness.[36,37]

In view of the above discussion, herein we have successfully synthesized yttrium oxide incorporated Pd-based electrocatalysts supported on reduced graphene oxide (rGO) and demonstrated that adding appropriate amount of yttrium to Pd based catalysts significantly increased the electrocatalytic performance during the formic acid electro-oxidation in acidic medium. The adjusted catalyst Pd_6Y_4/rGO exhibited enhanced electrocatalytic activity compared to reference catalyst (Pd/C and Pd/rGO).

Experimental section

Fabrication of reduced graphene oxides

A modified Hummer process was adopted to fabricate graphene oxide.[38] In a typical synthesis, 25 mL of concentrated H_2SO_4, $NaNO_3$ and graphite powder were added in 1 : 2 ratio and the mixture was agitated at a temperature below 10 °C for 30 minutes. The mixture was then gradually supplemented dropwise with $KMnO_4$ (3 g) that had been dissolved in distilled water (10 mL) in a separate flask. The temperature of the solution was lowered to 10 °C after 1 h of stirring at 35 °C. To the above mixture 100 mL of distilled water was added dropwise at constant temperature of 90 °C and stirred for 1 h. 35% H_2O_2 (5 mL) was added slowly afterwards. The resultant solution was cool down to room temperature before being rinsed many times with a 5% HCl solution. The blackish brown product (GO) was vacuum dried at 70 °C for 8 h. The synthesized GO was reduced to rGO by dispersing GO in distilled water having 1 mg mL^{-1} concentration and afterward added 2.5 mL of 65% hydrazine monohydrate and was kept for 2 h at 110 °C. The temperature of the resultant solution was lowered, filtered, and rinsed multiple times by deionized water and ethanol before being dried in a 70 °C oven for future use.

Synthesis of rGO supported yttrium oxide–palladium

The composite was fabricated using the sodium borohydride reduction method, with a total 20 wt% of the metal in the catalyst. In 20 mL distilled water 80 mg of rGO was uniformly dispersed by sonication for 1 h. Under normal stirring, the calculated amount of aqueous solution of yttrium nitrate hexahydrate was added dropwise. After being stirred for 30 minutes, calculated amount of palladium diacetate was added to the above mixture dropwise, while constantly agitating the solution. For the reduction of palladium and yttrium, freshly made sodium borohydride solution was injected drop by drop. The final product was separated by vacuum filtration, rinsed with ethanol and water, and dried at 60 °C. The fine powder was heated at 300 °C in reducing environment for 3 h to obtain Pd_yY_x/rGOs, where x and y signify the ratio of metals quantity and in the catalyst mixture. Pd/rGO and Pd/C catalysts were also fabricated as reference catalysts for comparison. Scheme 1 represents the synthesis of Pd_yY_x/rGOs.

Physical characterization

The synthesized catalyst and rGO were subjected to PXRD analysis using PANalytical version (Xpert Pro origin Netherlands) (=1.544206), which produced an X-ray diffraction pattern using Cu K radiation. The instruments operational parameters are 30 mA current, 40 kV potential, and 0.015 s^{-1} speed. By employing the model ESCALAB250Xi (Thermo Scientific, U. K.), with Al K having an energy of 1486.68 eV, X-ray photoelectron spectroscopy is used to evaluate the chemical compositions and valency of the metals in the catalyst. Fine detail about catalyst

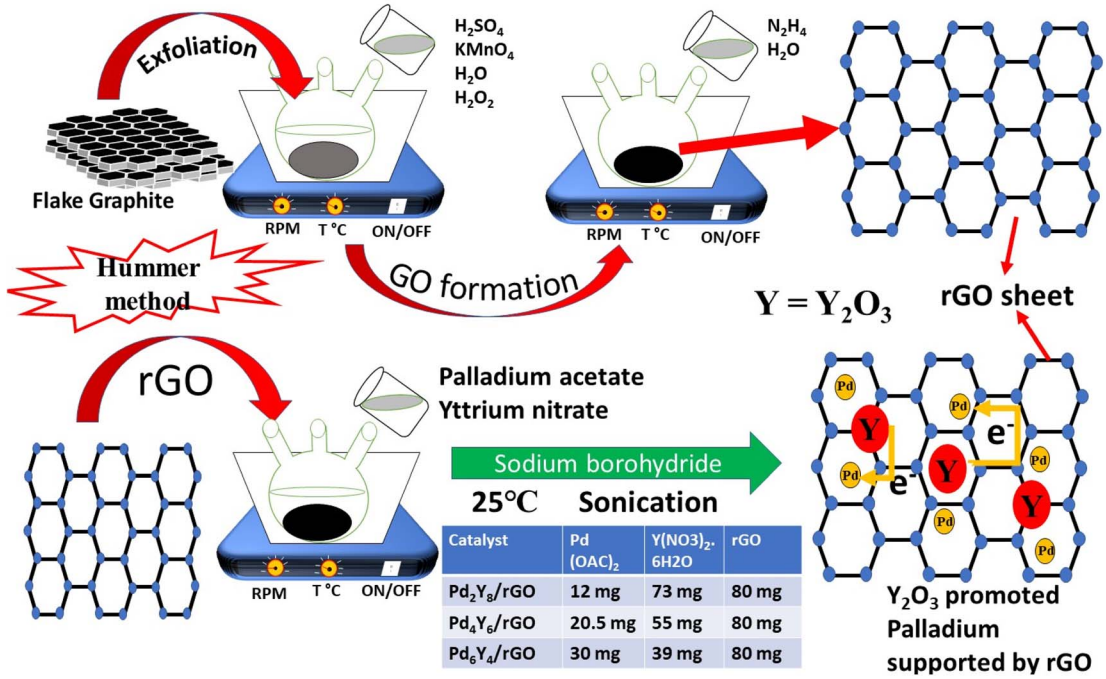

Catalyst	Pd $(OAC)_2$	$Y(NO3)_2$. 6H2O	rGO
Pd_2Y_8/rGO	12 mg	73 mg	80 mg
Pd_4Y_6/rGO	20.5 mg	55 mg	80 mg
Pd_6Y_4/rGO	30 mg	39 mg	80 mg

Scheme 1 Schematic representation for the synthesis Pd_yY_x/rGOs.

morphology was analyzed from 100 kV transmission electron microscopy on all the synthesized electrocatalysts using a Hitachi H-7700 model.

Atomic absorption spectroscopy (AAS) Shimadzu AA-670 Japan was used to determine the amount of metal in the catalysts.

Electrochemical investigation

The typical three electrode arrangement was used for all electrochemical tests. Working electrode was made by coating ink of the synthesized material on glassy carbon electrode. To prepare catalysts ink, 4 mg of each catalyst *i.e.*, Pd_yY_x/rGO was dispersed in solution (20 μL Nafion 117 binder and 180 μL isopropanol) to make a homogeneous slurry by sonicating it for 1 h. The ink of the synthesized catalysts each containing 0.0055 mg of Pd metal is allowed to dry on surface of glassy carbon electrode (0.071 cm^2). Counter electrode was graphite rod, the electrode used for reference was Ag/AgCl. A Biologic SP300 electrochemical workstation was used to conduct voltametric measurements. De-aeration of the solution was done for 20 minutes with ultrahigh-purity nitrogen gas. All electrochemical tests were conducted out in 1 M HCOOH and 0.5 M H_2SO_4 at room temperature. Catalyst activation was done by taking multi cycle in specific potential window (−0.25 to +0.25). Chronoamperometry test (*i vs. t*) was carried out at fixed potential (0.4 V) to check the prolonged stability and performance of the synthesized Pd_yY_x/rGO catalysts.

Result and discussion

Characterization

The crystal structure of synthesized materials was analyzed by PXRD measurements. Fig. S1† depicts the PXRD pattern of graphite, graphene oxide, and reduced graphene oxide. A prominent and condensed typical diffraction peak for GO was observed at $2\theta = 9.6°$. The vanishing of the typical peak at $2\theta = 9.6°$ of graphene oxide and presence of the wide peak at $2\theta = 25°$ (002) corresponding to reduced graphene oxide is the indication of successful transformation of GO into rGO.[39] The PXRD pattern of Pd_yY_x/rGOs illustrates broad diffraction peak which is attributed to (002) plane of carbon in the form of reduced graphene oxide at $2\theta = 24.8°$ (JCPDS 75-1621).[40] The peaks at $2\theta = 68°$,46.7° and 40° correspond to (220), (200) and (111) plane of fcc-Pd nanoparticles (JCPDS 00-001-1201) as shown in Fig. 2a. The diffraction peak for yttrium was not observed in the PXRD pattern of Pd_yY_x/rGO indicating the amorphous nature of yttrium.[41,42] Reference catalysts PXRD pattern is shown in Fig. S2.† Fig. S12† represents the pre and post CRD pattern of Pd_6Y_4/rGO.

Fig. 1 illustrates the X-rays photoelectron spectroscopy results of Pd_6Y_4/rGO to find out the oxidation states and chemical surroundings of the synthesized material. The carbon 1s XPS pre and post profile shows the appearance of four peaks at 284.6, 285.5, 288.3 and 286.4 eV for HO–C, C=C/C–C, O=C–OH and COOH/C=O bonds respectively (Fig. 1c).[43] The oxygen 1s profile has been shown in Fig. S14.† The peaks for Pd–O/HO–C=O, O=C, C–O and HO–C appears at binding energy values of ~531.3, 532.2, 534.6, and 533.7 eV respectively.[44]

The pre and post XPS profile of Pd 3d represents the appearance of two distinct peaks at 335.5 eV and 341.0 (Fig. 1e).[45] Fig. 1f represents the XPS profile of Y 3d ($3d_{5/2}$ and $3d_{3/2}$) peaks appear at 158.7 and 160.4 eV, respectively. These binding energy values suggest the presence of 3+ oxidation state of yttrium. The pre and post XPS survey pattern of the Pd_6Y_4/rGO electrocatalyst has been shown in Fig. S13.† Metal

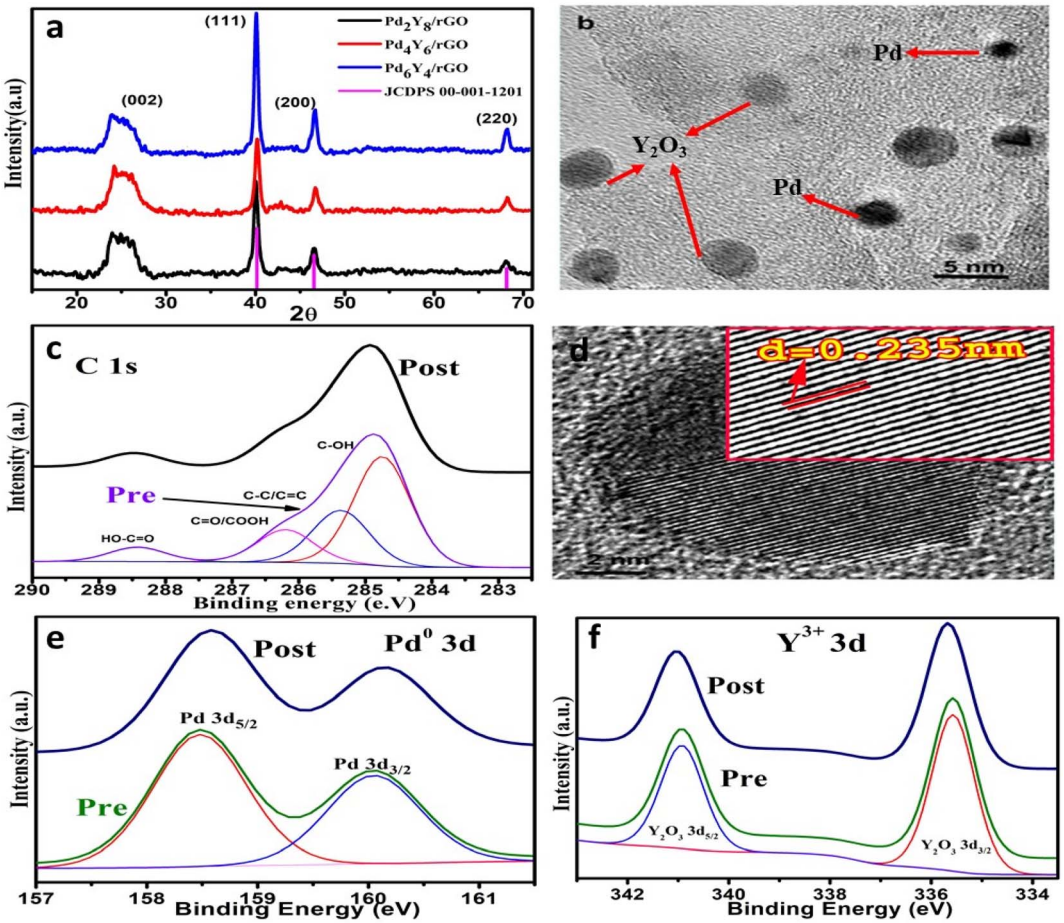

Fig. 1 (a) PXRD pattern of Pd_yY_x/rGOs (b) TEM images of Pd_6Y_4/rGO at 5 nm (c) pre and post XPS pattern of carbon (d) *d*-fringes of Pd in Pd_6Y_4/rGO (e) pre and post XPS pattern of palladium (f) pre and post XPS pattern of yttrium oxide.

concentration in all the synthesized electrocatalysts was determined by dissolving the 5 mg of the catalyst in 100 mL 7% HCL. The AAS data for all the synthesized electrocatalysts has been shown in Table S3.† The percentage of the metal was calculated and shown in Table S2.†

The SEM images of prepared rGOs (Fig. S3†) demonstrate the successful exfoliation of graphite to produce rGO which is also confirmed by PXRD pattern of rGO (Fig. S1†). By eliminating the functional groups of oxygen that were bonded to the edge and bottom plane of the graphene sheets, complete reduction of GO results in a bumpy and cracked surface. When all oxygen-containing functional groups are eliminated, rGO individual sheets are formed, which are randomly aggregated and have defined edges and wrinkled surfaces.[46–49] Fine details about morphology and structural features of the synthesized material were studied by TEM analysis at 5 nm. Palladium nanoparticles and yttrium oxide nanoparticles (NPs) are uniformly dispersed on the surface of the rGO sheets (Fig. 1b)[50]. On high surface area rGO support, the crystalline, spherical palladium nanoparticles of about ~5–10 nm size can be clearly seen in Fig. 1b. The calculated particle size from the TEM and XRD result match closely. Lattice fringes of 0.235 nm can be observed in HRTEM image which corresponds to (111) plane of Pd nanoparticles (Fig. 1d). Over the rGO nanosheets, two different kinds of particles are evenly scattered. Small black particles, evenly dispersed are made of palladium nanoparticles, whereas larger, more amorphous blur types of nanoparticles are made of yttrium oxide. TEM micrographs of Pd_6Y_4/rGO electrocatalyst at 10 and 20 nm resolution have been shown in Fig. S4.† TEM images of Pd_4Y_6/rGO and Pd_2Y_8/rGO is shown in Fig. S10.†

Electrochemical evaluation

To elaborate the electrochemical behavior of a catalyst, the determination of its electrochemical surface area is very important. Generally, catalyst having large value of electrochemical surface area (ECSA) have large number of active sites and thus it shows high electrochemical activities towards oxidation of small organic molecules.[51] The electrochemical surface area is typically determined by palladium oxide layer reduction method by recording cyclic voltametric (CV) curves in 0.5 M sulfuric acid. At 0.7 V, Pd oxidation occur. The signal around 0.65 V *vs.* Ag/AgCl in cathodic scan indicates the reduction of PdO. Additionally, compared to reference catalysts, the area under the peaks for PdO layer reduction was larger for Pd_6Y_4/rGO, which results from more electrochemically active

sites being present. By incorporating the area under the curve of PdO reduction, the electrocatalytically active surface area (ECSA) parameters of the Pd-based electrocatalysts were calculated.[52,53] The catalyst having composition Pd_6Y_4/rGO shows intense peak for palladium reduction in comparison to other synthesized catalysts. The electrochemical surface area of the catalyst is determined by applying the equation below.

$$\text{ECSA}\ \left(\text{m}^2\ \text{g}^{-1}\right) = \frac{Q_{\text{H}}}{420\ \mu\text{C} \times W}$$

where 420 μC cm^{-2} is the standard value of charge for Pd, Q_H is the value of integrated charge and W is metal loading on electrode surface. Table S1† show the calculated value of ECSA of all the synthesized electrocatalysts by Pd–O layer reduction method. The large surface area of Pd_6Y_4/rGO catalyst is due to wide dispersion of metal nanoparticles on reduced graphene oxide, small size of Pd nanoparticles and unform dispersion of Pd nanoparticles due to Y_2O_3 promotion.

Formic acid is electro-catalytically oxidized by two parallel reactions.[54,55] One route is indirect and comprises the production of CO* *via* dehydration of formic acid, which is further oxidized to CO_2. An oxygenated specie at the catalyst surface is needed for the oxidation of poisonous intermediate CO* which is produced during the reaction. As a result, a high voltage is needed for formic acid complete electro-oxidation.[56] The second method involves formic acid being directly oxidized to CO_2 without the formation of poisonous intermediate CO*.

The electrocatalytic activity of Pd_yY_x/rGOs for oxidation of formic acid was explored considering the unique advantages of using formic acid as a fuel and the capacity of Pd to catalyze the process *via* dehydrogenation route in 1 M formic acid 1 M HCOOH and 0.5 M sulfuric acid solution, at ambient temperature, with a sweep rate of 20 mV s^{-1}. The cyclic voltammogram of all the synthesized electrocatalysts were recorded between the potential range of −0.4 to +1 (Fig. 2a). The broad oxidation peak at ∼0.36 V, ∼0.38 V and ∼0.41 V for Pd_6Y_4/rGO, Pd_4Y_6/rGO, and Pd_2Y_8/rGO shows the oxidation of formic acid directly *via* dehydrogenation route respectively.[8] The production of the toxic intermediate *i.e.*; CO* during the dehydration route of formic acid oxidation results in the obstruction of the catalyst's active sites, which reduces the catalyst's efficiency and delays further formic acid oxidation.[57] In the cathodic scan from +1 to −0.4 V (Fig. 2a), the oxidation signal at ∼0.45, 0.40 and 0.69 V for Pd_6Y_4/rGO, Pd_4Y_6/rGO and Pd_2Y_8/rGO are attributed to the dehydration process in the oxidation of formic acid respectively. Current density is obtained when the current is scaled to the electrode's geometric surface area. ThePd_6Y_4/rGO delivers the highest current density of 106.60 mA cm^{-2} among all the synthesized electrocatalysts (Fig. 2a).

The oxidation peak current density of catalysts consisting of yttrium oxide in palladium, exhibits roughly a several fold increase, proving that the presence of yttrium oxide in catalyst has increased intrinsic catalytic activity. The current density of Pd_6Y_4/rGO shows approximately 3.7-fold and 4.9-fold increase than the Pd/rGO and Pd/C (Fig. S5†). Table S1† represents the current density values of all the synthesized electrocatalysts. The mass specific activity is obtained when current is normalized to palladium mass loaded on the electrode. The mass specific activity for Pd_yY_x/rGOs electrocatalysts has been shown in Fig. 2b. Among all the synthesized electrocatalysts, Pd_6Y_4/

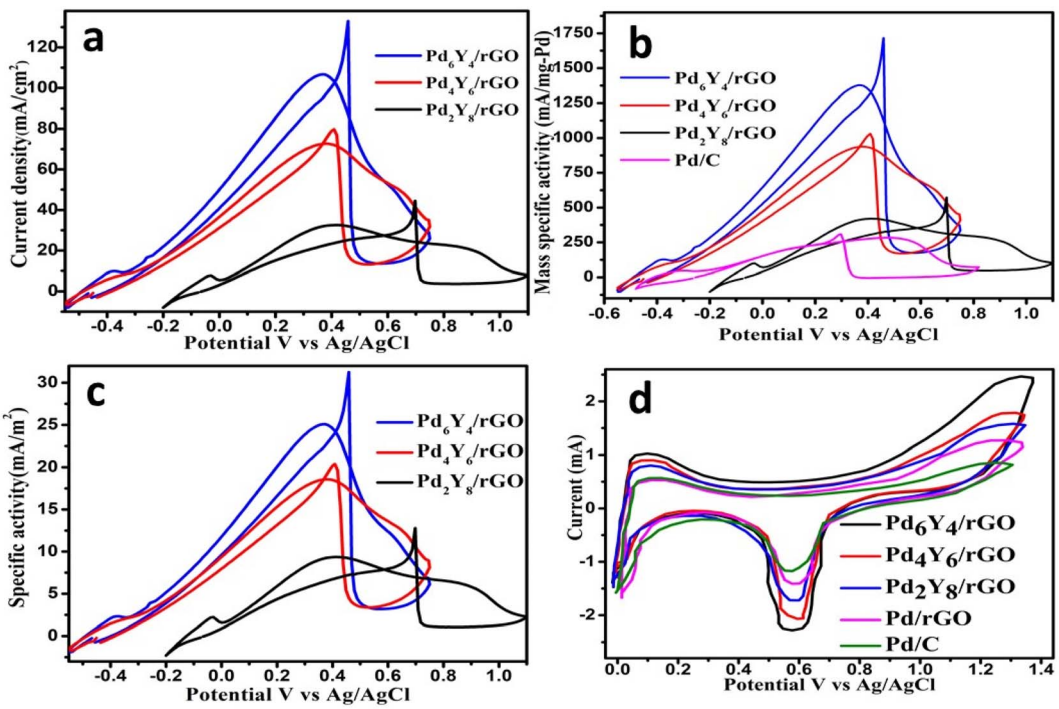

Fig. 2 CV parameters of catalysts for FAO in 0.5 M H_2SO_4 and 1 M HCOOCH (a) current density of Pd_xY_y/rGOs catalysts (b) mass specific activity of Pd_yY_x/rGOs catalyst and Pd/C (c) specific activity of Pd_xY_y/rGOs catalysts (d) CV curves of catalysts in 0.5 M H_2SO_4.

rGO gives the high value of mass specific activity of about 1380 mA mg_{Pd}^{-1} which is about 3.74 and 4.82 time higher than the Pd/rGO and Pd/C respectively. When current is normalized to electrochemical surface area of catalyst it gives specific activity (Fig. 2c). Specific activity of Pd_6Y_4/rGO electrocatalyst is 11.55 mA m^{-2} which is 1.3, 2.6, 2.5 and 3.2 times higher than that of Pd_4Y_6/rGO, Pd_2Y_8/rGO, Pd/rGO and Pd/C respectively. Table S1† represents the mass specific activity and specific activity values for all synthesized electrocatalysts. Fig. S6 and S7† show comparison of reference catalysts (Pd/C and Pd/rGO) with the synthesized final electrocatalyst (Pd_6Y_4/rGO) in terms of mass specific activity and specific activity during formic acid electrochemical oxidation.

The shifting of oxidation peak potential to lower value demonstrates the higher resistance of the synthesized catalyst (Pd_6Y_4/rGO) towards the CO adsorption.[58] When compared to reference catalysts, the oxidation potential for Pd_6Y_4/rGO was moved by 110 mV towards negative side (Fig. S8†), demonstrating that Pd_6Y_4/rGO has outstanding response towards formic acid oxidation.[36]

As a measure of an electrocatalyst tolerance ability towards carbonaceous species (CO_{ads}) produced during oxidation of formic acid, the ratio of oxidation peak current (forward to backward scan) is used. Smaller the ratio, larger will be the tolerance ability towards toxic intermediates produced during the reaction. The ratio for Pd_6Y_4/rGO is 0.80 which is smaller than reference catalysts (Pd/rGO ~ 0.93 and Pd/C ~ 0.87) showing the highest tolerance ability.[59]

The Tafel slope, which can be obtained by linear fitting of the data plotted *versus* log *j* and voltage under the very low current polarization circumstances, is another parameter for evaluating the intrinsic performance of the electrocatalyst towards the formic acid oxidation.[60,61] Tafel slope analysis can be used to study the catalytic mechanism. As illustrated in Fig. 3c, the Tafel slope was calculated by recording the quasi-static measurement of linear sweep voltammetry with a low sweep step of 5 mV s^{-1}. Between 0.00 and 0.35 V, Tafel slope was estimated. According to the measurements, the Tafel slopes for Pd_6Y_4/rGO, Pd/rGO and Pd/C respectively, are 281, 413, 470 mV dec^{-1}. Different Tafel slope values represent various catalytic mechanisms and the quantity of adsorbed reactants in the catalytic process. As dehydrogenation is the rate-determining step (RDS) through CO_2 generation, the lowest Tafel slope value designates the principal route and evidences the improved dehydrogenation primarily because there are fewer toxic species.[62] The small Tafel slope value of Pd_6Y_4/rGO (281 mV dec^{-1}), confirms that the catalytic mechanism proceeds *via* direct channel or dehydrogenation (Fig. 3c). The rate of charge transfer of the Pd_6Y_4/rGO catalyst for the formic acid electrochemical oxidation of formic acid is obviously quicker and have the highest intrinsic catalytic activity as shown by the small value of Tafel slope with quicker electron transmission and active species movement.

Resistance to charge transfer during formic acid electrochemical oxidation was measured using electrochemical impedance spectroscopy. Fig. 3b displays the Nyquist plots for Pd_yY_x/rGOs and reference catalysts in 1 M H_2CO_2 and 0.5 M H_2SO_4 solution between 1 KHz and 10 MHz at a specific potential of 0.30 V at 25 °C. The radius of the extended semicircle, which corresponds to the polarization resistance of the electrolytic cell in the Nyquist diagram, significantly controls

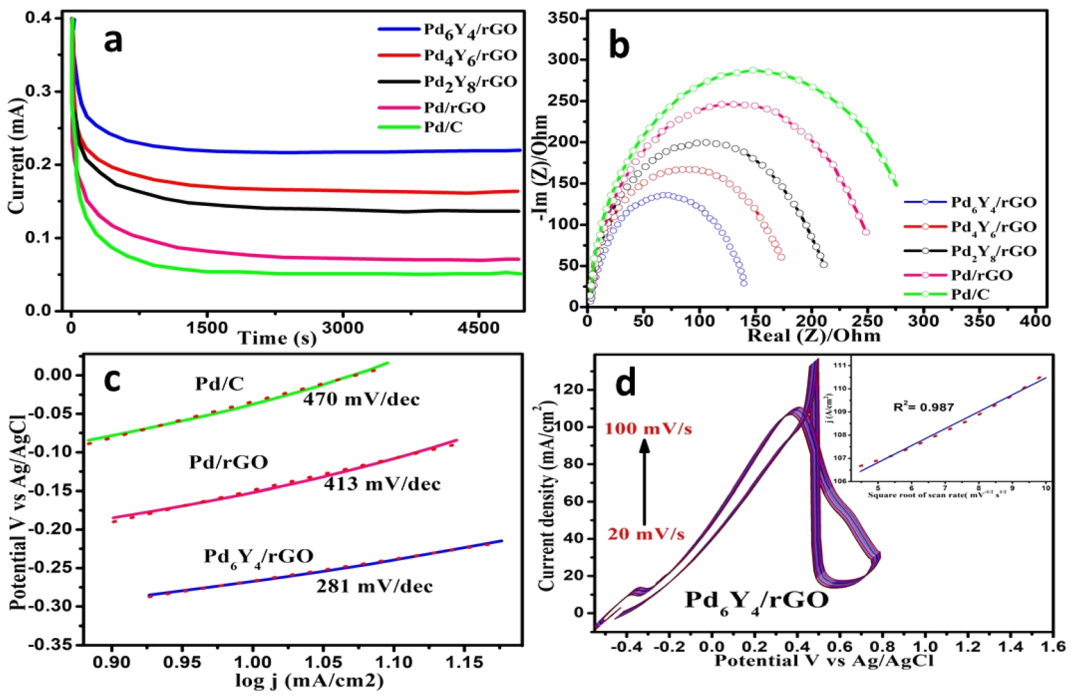

Fig. 3 (a) Current *vs.* time profile of Pd_xY_y/rGOs and reference catalysts (b) Nyquist profile of Pd_xY_y/rGOs and reference catalysts (c) Tafel slope of Pd_6Y_4/rGO and reference catalysts (d) transport characteristics of Pd_6Y_4/rGO.

the charge transfer resistance. Smaller charge transfer resistance (R_{ct}) and subsequently greater oxidation kinetics are derived from smaller semicircle diameter.[63,64] When compared to the other catalysts, the Pd_6Y_4/rGO has the lowest R_{ct} (~135 Ω) showing a fast reaction kinetics towards formic acid oxidation. The comparative result indicates that the Pd based electrocatalyst with optimized ratio between Pd and Y (Pd_6Y_4/rGO) probably promotes the quick charge transference at the electrode/electrolyte junction. Table S1† represents the R_{ct} values of all the synthesized electrocatalysts.

The standard exchange current density (i_0), based on the value of R_{ct}, is another parameter in assessing the electrocatalytic activity of a catalyst in addition to the onset potentials.[65] The value of i_0 can be found from this equation

$$R_{ct} = \frac{RT}{nFi_0}$$

where, R is gas constant F is Faraday constant and n is the number of electrons associated in oxidation reaction. From above equation the value of i_0 is in the order, Pd_6Y_4/rGO (7.9×10^{-6} A cm^{-2}) > Pd_4Y_6/rGO (6.3×10^{-6} A cm^{-2}) > Pd_2Y_8/rGO (5.1×10^{-6} A cm^{-2}) > Pd/rGO (4.2×10^{-6} A cm^{-2}) > Pd/C (3.8×10^{-6} A cm^{-2}). The value of exchange current density is higher for Pd_6Y_4/rGO showing highest intrinsic electrocatalytic performance during formic acid electrochemical oxidation.

Another important parameter for electrocatalysts is its long-term catalytic stability.[66] Using chronoamperometry (CA), the synthesised materials' long-term stability during the oxidation of formic acid was evaluated which is depicted in Fig. 3a. To compare the stability of the catalyst, CA experiment was run for 5000 s in solution of (1 M formic acid and 0.5 M sulfuric acid) purged with N_2 at a fixed potential of 0.4 V. Initially all catalysts showed a higher current, which was explained by the lot of active sites present on their region. Value of current density steadily decreased in the first 1200 s for all catalyst following the formation and adsorption of the CO_{ads} intermediate species on the catalyst active sites *via* oxidation.[19] Surprisingly, over the course of the entire experimental testing period, after 5000 seconds, the Pd_6Y_4/rGO catalyst retained the highest final current density (70%), followed by Pd_4Y_6/rGO (53%), Pd_2Y_8/rGO (43%) and reference catalyst (Pd/rGO 23% and Pd/C 16%). This indicates that the Pd_6Y_4/rGO catalyst exhibits highest catalytic performance and durability, along with a strong CO* tolerance. The fact that the Pd_6Y_4/rGO bimetallic electrocatalyst exhibits exceptional stability and catalytic response during the formic acid oxidation is significant because it supports the benefits of using Pd nanoparticles promoted by Y_2O_3 nanoparticles on rGO, which show high tolerance to CO* poisoning. In this situation, Y_2O_3 nanoparticles boost the current density while simultaneously enhancing the stability by increasing the CO-tolerance ability of catalysts. The stability of the catalyst and the potential for the oxidation process were both influenced by the addition of Y_2O_3. Therefore, the catalytic system containing Pd and Y_2O_3 may be a suitable and effective catalyst for electrochemical oxidation of formic acid reaction in fuel cells. The electrochemical activity of the material after the chronoamperometric measurements has been shown in the Fig. S11.†

Fuel delivery to the reaction sites becomes incredibly slow if the kinetics of the anodic pathway is sluggish, which leads to starvation of fuel on the anode side.[67] In order to investigate the impact of various scan rates on the electrochemical behaviour of the Pd_6Y_4/rGO electrode during oxidation of formic acid, the transport properties of catalysts were analysed (Fig. 3d). The increase in scan rate shifts the oxidation of formic acid towards more positive value and increases the electrocatalytic peak current (Fig. S9†). The transport characteristics of the Pd_6Y_4/rGO electrode are determined by relating square root value of scan rate ($v^{1/2}$) to the forward peak current (i_f). The anodic peak current (i_p) was associated with the scan rate *via* equation in accordance with the quasi-linear diffusion precondition:

$$i_p = (2.99 \times 10^5)\, n^{3/2} C_o D_o V^{1/2}$$

Table 1 Comparison of electrochemical performance of reported literature and the current work

Catalysts	[a]ECSA (m^2 g^{-1})	[b]E_f	[c]E_r	[d]J_m (mA cm^{-2})	[e]J_m (mA cm^{-2})	[f]J_m (mA mg^{-1} Pd)	[g]SA (mA cm^{-2})	Ref.
$Pd_{75}Cu_{25}$/N-rGO	73.39	0.139	0.40	88.7	61.8	1738	2.4	69
7% Pd/cubes CeO_2/C	93.02	0.2	0.3	16	15	1059.18	11.38	70
$Pd_{15}Pt_1$/15CeO_2–C	—	0.08	0.18	18.5	15	740	—	28
Pd_3/CuO-10CNT	32.41	0.28	0.27	28	26	1904	26.9	44
Pd_1Ni1-NNs/RGO	98.2	0.28	0.3	—	—	604	6.1	71
Pd–15%NiO-CNT	49.56	0.32	0.42	80	70	640	12.9	31
Pd/1N-CQDs-SiO_2-1rGO	52.9	0.115	0.15	38.7	21.6	905	12.81	44
$PdEuO_x$/C	102/70	0.33	0.34	70	—	740	0.74	32
Pd/SnO_2–S	79.51	0.121	0.20	22.3	21	637	8.01	72
Pd_6Y_4/rGO	119.4	0.36	0.46	106.6	132.95	1380	11.55	This work
Pd_4Y_6/rGO	107.73	0.38	0.41	73.02	79.61	939.32	8.63	This work
Pd_2Y_8/rGO	96.05	0.127	0.41	32.48	44.63	410.84	4.3	This work
Pd/rGO	80.78	0.43	0.271	28.36	30.51	368.16	4.5	This work
Pd/C	76.88	0.51	0.291	21.70	24.04	285.73	3.6	This work

[a] ECSA was measured from PdO reduction method. [b] Forward peak potential. [c] Backward peak potential. [d] Forward current density. [e] Backward current density. [f] Forward mass specific activity. [g] Specific activity.

where substrate bulk concentration is C_o, diffusion quantity is D_o, electrode surface area is A, electrons transferred number is n, i_p is peak current and $v^{1/2}$ is square rooted value of scan rate. If C_o is kept fixed, peak current (i_p) is directly related to ($v^{1/2}$). Diffusion-controlled response has been shown in Fig. 3d (inset) when i_p, and $v^{1/2}$ is directly related.[68] The formic acid oxidation process on the Pd_6Y_4/rGO electrode is regulated by diffusion because of the correlation coefficient, $R^2 = 0.987$ (inset in Fig. 3d).[67]

Reduced graphene oxide supported, and yttrium oxide promoted palladium based electrocatalysts electrochemical performance during formic acid oxidation was related to the reported values of other Pd-based electrocatalysts promoted by transition metal oxide in the literature (Table 1). Compared to all other Pd-based catalysts, Pd_6Y_4/rGO shown highest current density and large ECSA and current density. On addition of Y_2O_3 to Pd nanomaterial the electrocatalytic activities towards formic acid oxidation have been enhanced due to following reasons.

(1) Y_2O_3 causes uniform dispersion of Pd nanoparticles.

(2) Stops agglomeration and thus exposing more active sites of Pd nanoparticles.

(3) Lowers the d-band center of palladium.

(4) Decreases the binding strength of the reactive intermediate.

The electrocatalytic activities for the oxidation of formic acid were also significantly impacted by the presence of graphene due to its conductivity and ionic conductivity through reduced graphene oxide to Pd.

Conclusions

For the formic acid oxidation in an acidic solution, the as-prepared catalyst (Pd_yY_x/rGOs), synthesized by sodium borohydride reduction method, outperformed the Pd/C and Pd/rGO catalysts in terms of electrocatalytic activity. The small size palladium nanoparticles were uniformly dispersed on highly conductive rGO support. The catalyst's metallic ratio of palladium metal to yttrium oxide was carefully adjusted to achieve maximum catalytic activity. The outcomes demonstrated that Y_2O_3 significantly influenced the electrocatalytic activities for the oxidation of formic acid. All of the findings indicate that adding Y_2O_3 nanoparticles improve the catalyst stability and activity for formic acid electrooxidation. The strong interaction between the tiny and uniformly sized Pd and Y_2O_3 nanoparticles and the rGO support, is the reason for the catalytic improvement. The Pd_6Y_4/rGO catalyst performs best in terms of stability and catalytic activity with total metal content of 20 wt%.

Conflicts of interest

There are no conflicts to declare.

Acknowledgements

The work was financially supported by the Pakistan Academy of Sciences (PAS) and Higher Education Commission (HEC) of Pakistan (No. 8400/Federal/NRPU/R&D/HEC/2017).

References

1 S.-Y. Wu and H.-T. Chen, Electrochemical formic acid oxidation catalyzed by graphene supported bimetallic Pd-Ni clusters: the role of Ni content and the hydrogen coverage effect, *Appl. Surf. Sci.*, 2022, **606**, 154944.

2 Z. Ai, B. Chang, C. Xu, B. Huang, Y. Wu, X. Hao and Y. Shao, Interface engineering in the BNNS@ Ti_3C_2 intercalation structure for enhanced electrocatalytic hydrogen evolution, *New J. Chem.*, 2019, **43**(22), 8613–8619.

3 X. Xu, J. Tang, Y. V. Kaneti, H. Tan, T. Chen, L. Pan, T. Yang, Y. Bando and Y. Yamauchi, Unprecedented capacitive deionization performance of interconnected iron–nitrogen-doped carbon tubes in oxygenated saline water, *Mater. Horiz.*, 2020, **7**(5), 1404–1412.

4 H. Huang, M. Yan, C. Yang, H. He, Q. Jiang, L. Yang, Z. Lu, Z. Sun, X. Xu and Y. Bando, Graphene nanoarchitectonics: recent advances in graphene-based electrocatalysts for hydrogen evolution reaction, *J. Adv. Mater.*, 2019, **31**(48), 1903415.

5 X. Xu, T. Yang, Q. Zhang, W. Xia, Z. Ding, K. Eid, A. M. Abdullah, M. S. A. Hossain, S. Zhang and J. Tang, Ultrahigh capacitive deionization performance by 3D interconnected MOF-derived nitrogen-doped carbon tubes, *J. Chem. Eng.*, 2020, **390**, 124493.

6 Z. Wang, X. Xu, J. Kim, V. Malgras, R. Mo, C. Li, Y. Lin, H. Tan, J. Tang and L. Pan, Nanoarchitectured metal–organic framework/polypyrrole hybrids for brackish water desalination using capacitive deionization, *Mater. Horiz.*, 2019, **6**(7), 1433–1437.

7 E. Plaza-Mayoral, I. J. Pereira, K. N. Dalby, K. D. Jensen, I. Chorkendorff, H. Falsig, P. Sebastián-Pascual and M. Escudero-Escribano, Pd-Au nanostructured electrocatalysts with tunable compositions for formic acid oxidation, *ACS Appl. Energy Mater.*, 2022, 1–13.

8 I. A. Khan, M. Sofian, A. Badshah, M. A. Khan, M. Imran and M. A. Nadeem, Stable and efficient PtRu electrocatalysts supported on Zn-BTC MOF derived microporous carbon for formic acid fuel cells application, *Inorg. Chem. Front.*, 2020, **8**, 367.

9 N. Li, Preparation of FePd-RGO Bimetallic Composites with High Catalytic Activity for Formic Acid Electro-Oxidation, *Chin. J. Chem.*, 2016, **34**(11), 1129–1134.

10 J. Xu, M. Zhao, S.-i. Yamaura, T. Jin and N. Asao, Core–shell Pd–P@ Pt nanoparticles as efficient catalysts for electrooxidation of formic acid, *J. Appl. Electrochem.*, 2016, **46**(11), 1109–1118.

11 D. Liu, M. Xie, C. Wang, L. Liao, L. Qiu, J. Ma, H. Huang, R. Long, J. Jiang and Y. Xiong, Pd-Ag alloy hollow nanostructures with interatomic charge polarization for enhanced electrocatalytic formic acid oxidation, *Nano Res.*, 2016, **9**(6), 1590–1599.

12 Z. Fang and W. Chen, Recent advances in formic acid electro-oxidation: From the fundamental mechanism to electrocatalysts, *Nanoscale Adv.*, 2021, **3**(1), 94–105.

13 Z. Ma, U. Legrand, E. Pahija, J. R. Tavares and D. C. Boffito, From CO_2 to formic acid fuel cells, *Ind. Eng. Chem. Res.*, 2020, **60**(2), 803–815.

14 Y. Zhou, D. Liu, Z. Liu, L. Feng and J. Yang, Interfacial Pd–O–Ce linkage enhancement boosting formic acid electrooxidation, *ACS Appl. Mater. Interfaces*, 2020, **12**(41), 47065–47075.

15 L. Liang, F. Vladimir, J. Ge, C. Liu and W. Xing, Highly active PtAu alloy surface towards selective formic acid electrooxidation, *J. Energy Chem.*, 2019, **37**(1), 157–162.

16 T. J. Wang, Y. C. Jiang, J. W. He, F. M. Li, Y. Ding, P. Chen and Y. Chen, Porous palladium phosphide nanotubes for formic acid electrooxidation, *Carbon Energy*, 2022, **4**(3), 283–293.

17 P. N. Duchesne, Z. Li, C. P. Deming, V. Fung, X. Zhao, J. Yuan, T. Regier, A. Aldalbahi, Z. Almarhoon and S. Chen, Golden single-atomic-site platinum electrocatalysts, *Nat. Mater.*, 2018, **17**(11), 1033–1039.

18 Z. Guo, X. Kang, X. Zheng, J. Huang and S. Chen, PdCu alloy nanoparticles supported on CeO_2 nanorods: Enhanced electrocatalytic activity by synergy of compressive strain, PdO and oxygen vacancy, *J. Catal.*, 2019, **374**, 101–109.

19 S. Saipanya, L. Fang, S. Themsirimongkon, S. Maturost, N. Pongpichayakul, N. Promsawan and P. Waenkaew, Polyvinyl alcohol-modified graphene oxide as a support for bimetallic Pt–Pd electrocatalysts to enhance the efficiency of formic acid oxidation, *Polym. Adv. Technol.*, 2022, **33**(1), 120–133.

20 D. Rajesh, C. Mahendiran and C. Suresh, The Promotional Effect of Ag in Pd-Ag/Carbon Nanotube-Graphene Electrocatalysts for Alcohol and Formic Acid Oxidation Reactions, *ChemElectroChem*, 2020, **7**(12), 2629–2636.

21 T. Shen, S. Chen, R. Zeng, M. Gong, T. Zhao, Y. Lu, X. Liu, D. Xiao, Y. Yang and J. Hu, Tailoring the antipoisoning performance of Pd for formic acid electrooxidation via an ordered PdBi intermetallic, *ACS Catal.*, 2020, **10**(17), 9977–9985.

22 F. Luo, Q. Zhang, X. Yu, S. Xiao, Y. Ling, H. Hu, L. Guo, Z. Yang, L. Huang and W. Cai, Palladium phosphide as a stable and efficient electrocatalyst for overall water splitting, *Angew. Chem., Int. Ed.*, 2018, **57**(45), 14862–14867.

23 Z. Xi, D. P. Erdosy, A. Mendoza-Garcia, P. N. Duchesne, J. Li, M. Muzzio, Q. Li, P. Zhang and S. Sun, Pd nanoparticles coupled to WO2. 72 nanorods for enhanced electrochemical oxidation of formic acid, *Nano Lett.*, 2017, **17**(4), 2727–2731.

24 Z. Teng, M. Li, Z. Li, Z. Liu, G. Fu and Y. Tang, Facile synthesis of channel-rich ultrathin palladium-silver nanosheets for highly efficient formic acid electrooxidation, *Mater. Today Energy*, 2021, **19**, 100596.

25 H.-H. Wang, J.-F. Zhang, Z.-L. Chen, M.-M. Zhang, X.-P. Han, C. Zhong, Y.-D. Deng and W.-B. Hu, Size-controllable synthesis and high-performance formic acid oxidation of polycrystalline Pd nanoparticles, *Rare Met.*, 2019, **38**(2), 115–121.

26 H. Kivrak, S. Khalid, A. Caglar, D. Alpaslan, K. Selcuk, T. E. Dudu and N. Aktas, The preparation, characterization, and electrooxidation of colloidal palladium modified poly (methacrylic acid) hydrogel as formic acid fuel cell anode catalyst, *J. Energy Storage*, 2022, **4**(1), e286.

27 D.-M. Gu, Y.-Y. Chu, Z.-B. Wang, Z.-Z. Jiang, G.-P. Yin and Y. Liu, Methanol oxidation on Pt/CeO_2–C electrocatalyst prepared by microwave-assisted ethylene glycol process, *Appl. Catal., B*, 2011, **102**(1–2), 9–18.

28 L. Yang, H. Su, T. Shu and S. Liao, Enhanced electro-oxidation of formic acid by a PdPt bimetallic catalyst on a CeO_2-modified carbon support, *Sci. China Chem.*, 2012, **55**(3), 391–397.

29 A. Bulut, M. Yurderi, Y. Karatas, Z. Say, H. Kivrak, M. Kaya, M. Gulcan, E. Ozensoy and M. Zahmakiran, MnO_x-promoted PdAg alloy nanoparticles for the additive-free dehydrogenation of formic acid at room temperature, *ACS Catal.*, 2015, **5**(10), 6099–6110.

30 S. Maturost, S. Themsirimongkon, S. Saipanya, L. Fang, N. Pongpichayakul, J. Jakmunee and P. Waenkaew, Carbon nanotube-copper oxide-supported palladium anode catalysts for electrocatalytic enhancement in formic acid oxidation, *Int. J. Hydrogen Energy*, 2022, **47**(8), 5585–5598.

31 S. Hossain, J. Saleem, A. A. Ahmed, M. Hossain, M. Shaikh, S. Rahman and G. Mc Kay, Preparation and evaluation of nickel oxide-carbon nanotube supported palladium as anode electrocatalyst for formic acid fuel cells, *Int. J. Electrochem. Sci.*, 2016, **11**, 2686–2708.

32 L. Feng, S. Yao, X. Zhao, L. Yan, C. Liu and W. Xing, Electrocatalytic properties of Pd/C catalyst for formic acid electrooxidation promoted by europium oxide, *J. Power Sources*, 2012, **197**, 38–43.

33 B. Abraham, K. Maniam, A. Kuniyil and R. Chetty, Electrocatalytic performance of palladium dendrites deposited on titania nanotubes for formic acid oxidation, *Fuel Cells*, 2016, **16**(5), 656–661.

34 L. Y. Zhang, C. X. Guo, H. Pang, W. Hu, Y. Qiao and C. M. Li, DNA-Promoted Ultrasmall Palladium Nanocrystals on Carbon Nanotubes: Towards Efficient Formic Acid Oxidation, *ChemElectroChem*, 2014, **1**(1), 72–75.

35 M. J. Lázaro, S. Ascaso, S. Pérez-Rodríguez, J. C. Calderón, M. E. Gálvez, M. J. Nieto, R. Moliner, A. Boyano, D. Sebastián and C. Alegre, Carbon-based catalysts: Synthesis and applications, *C. R. Chim.*, 2015, **18**(11), 1229–1241.

36 C. Ray, S. Dutta, R. Sahoo, A. Roy, Y. Negishi and T. Pal, Fabrication of Nitrogen-Doped Mesoporous-Carbon-Coated Palladium Nanoparticles: An Intriguing Electrocatalyst for Methanol and Formic Acid Oxidation, *Chem.–Asian J.*, 2016, **11**(10), 1588–1596.

37 D. Shi, B. Chang, Z. Ai, H. Jiang, F. Chen, Y. Shao, J. Shen, Y. Wu and X. Hao, Boron carbonitride with tunable B/N Lewis acid/base sites for enhanced electrocatalytic overall water splitting, *Nanoscale*, 2021, **13**(5), 2849–2854.

38 U. Shamraiz, Z. Ahmad, B. Raza, A. Badshah, S. Ullah and M. A. Nadeem, CaO-promoted graphene-supported palladium nanocrystals as a universal electrocatalyst for

direct liquid fuel cells, *ACS Appl. Mater. Interfaces*, 2020, **12**(4), 4396–4404.

39 M. Fang, Z. Wang, X. Chen and S. Guan, Sponge-like reduced graphene oxide/silicon/carbon nanotube composites for lithium ion batteries, *Appl. Surf. Sci.*, 2018, **436**, 345–353.

40 C. Goswami, H. Saikia, K. Tada, S. Tanaka, P. Sudarsanam, S. K. Bhargava and P. Bharali, Bimetallic palladium–nickel nanoparticles anchored on carbon as high-performance electrocatalysts for oxygen reduction and formic acid oxidation reactions, *ACS Appl. Energy Mater.*, 2020, **3**(9), 9285–9295.

41 H. Ali, F. K. Kanodarwala, I. Majeed, J. A. Stride and M. A. Nadeem, La2O3 Promoted Pd/rGO electro-catalysts for formic acid oxidation, *ACS Appl. Mater. Interfaces*, 2016, **8**(47), 32581–32590.

42 Y. Yang, L. Wang, A. Li, Z. Jia, Y. Wang and T. Qi, Novel palladium–yttrium (Pd–Y/C) catalysts for methanol electrooxidation in alkaline media, *J. Solid State Electrochem.*, 2015, **19**, 923–927.

43 R. Cong, J.-Y. Choi, J.-B. Song, M. Jo, H. Lee and C.-S. Lee, Characteristics and electrochemical performances of silicon/carbon nanofiber/graphene composite films as anode materials for binder-free lithium-ion batteries, *Sci. Rep.*, 2021, **11**(1), 1–11.

44 S. Saipanya, P. Waenkaew, S. Maturost, N. Pongpichayakul, N. Promsawan, S. Kuimalee, O. Namsar, K. Income, B. Kuntalue and S. Themsirimongkon, Catalyst Composites of Palladium and N-Doped Carbon Quantum Dots-Decorated Silica and Reduced Graphene Oxide for Enhancement of Direct Formic Acid Fuel Cells, *ACS Omega*, 2022, **7**(21), 17741–17755.

45 S. Gao, S. Hu, G. Luo, S. Sun and X. Zhang, 2, 2′-bipyridine palladium(II) complexes derived N-doped carbon encapsulated palladium nanoparticles for formic acid oxidation, *Electrochim. Acta*, 2022, **413**, 140179.

46 S. Elbasuney, G. S. El-Sayyad, H. Tantawy and A. H. Hashem, Promising antimicrobial and antibiofilm activities of reduced graphene oxide-metal oxide (RGO-NiO, RGO-AgO, and RGO-ZnO) nanocomposites, *RSC Adv.*, 2021, **11**(42), 25961–25975.

47 F. Mindivan, The synthesis and charecterization of graphene oxide (GO) and reduced graphene oxide (rGO), *Mach., Technol., Mater.*, 2016, **10**(6), 32–35.

48 C. P. P. Wong, C. W. Lai, K. M. Lee and S. B. Abd Hamid, Advanced chemical reduction of reduced graphene oxide and its photocatalytic activity in degrading reactive black 5, *Materials*, 2015, **8**(10), 7118–7128.

49 B. K. Kuila, S. M. Zaeem, S. Daripa, K. Kaushik, S. K. Gupta and S. Das, Mesoporous Mn_3O_4 coated reduced graphene oxide for high-performance supercapacitor applications, *Mater. Res. Express*, 2018, **6**(1), 015037.

50 P. Chandran, A. Ghosh and S. Ramaprabhu, High-performance Platinum-free oxygen reduction reaction and hydrogen oxidation reaction catalyst in polymer electrolyte membrane fuel cell, *Sci. Rep.*, 2018, **8**(1), 1–11.

51 L. Y. Zhang, Y. Ouyang, S. Wang, Y. Gong, M. Jiang, W. Yuan and C. M. Li, Ultrafast synthesis of uniform 4–5 atoms-thin layered tremella-like Pd nanostructure with extremely large electrochemically active surface area for formic acid oxidation, *J. Power Sources*, 2020, **447**, 227248.

52 L. Y. Zhang, Y. Gong, D. Wu, G. Wu, B. Xu, L. Bi, W. Yuan and Z. Cui, Twisted palladium–copper nanochains toward efficient electrocatalytic oxidation of formic acid, *J. Colloid Interface Sci.*, 2019, **537**, 366–374.

53 Z. L. Z. Z. Li, Formic Acid-Reduced Ultrasmall Pd Nanocrystals on Graphene to Provide Superior Electrocatalytic Activity and Stability toward Formic Acid Oxidation, *Nano Energy*, 2015, **11**, 71–77.

54 Z. Fang and W. Chen, Recent advances in formic acid electro-oxidation: from the fundamental mechanism to electrocatalysts, *Nanoscale Adv.*, 2021, **3**(1), 94–105.

55 P. Zhang, X. Dai, X. Zhang, Z. Chen, Y. Yang, H. Sun, X. Wang, H. Wang, M. Wang and H. Su, One-pot synthesis of ternary Pt–Ni–Cu nanocrystals with high catalytic performance, *J. Mater. Chem.*, 2015, **27**(18), 6402–6410.

56 A. Gharib and A. Arab, Electrodeposited Pd, PdCd, and PdBi nanostructures: preparation, characterization, corrosion behavior, and their electrocatalytic activities for formic acid oxidation, *J. Electroanal. Chem.*, 2020, **866**, 114166.

57 X. Li, Y. Sun, C. Shen, Z. Zheng, H. Chen, Y. Jiang and Z. Xie, Heterogeneous fcc-Pt/hcp-PtBi Thick-Edge Nanoplates with Enhanced Activity for Formic Acid Oxidation, *ACS Appl. Energy Mater.*, 2021, **4**(9), 9190–9197.

58 J. Xie, D. Huang, H. Yin, F. Liu and Y. Ding, Au-Stabilized Nanoporous PdCuAu Alloys Exhibiting Outstanding Catalytic Activity and Durability for the Formic Acid Oxidation Reaction, *ACS Appl. Mater. Interfaces*, 2022, **14**(31), 35466–35476.

59 S. Mondal and C. R. Raj, Electrochemical dealloying-assisted surface-engineered Pd-based bifunctional electrocatalyst for formic acid oxidation and oxygen reduction, *ACS Appl. Mater. Interfaces*, 2019, **11**(15), 14110–14119.

60 S. Kumar, R. Soni and S. Kurungot, PdP/WO_3 multi-functional catalyst with high activity and stability for direct liquid fuel cells (DLFCs), *Sustainable Energy Fuels*, 2021, **5**(18), 4758–4770.

61 N. Wang, B. Tao, F. Miao and Y. Zang, Electrodeposited Pd/graphene/ZnO/nickel foam electrode for the hydrogen evolution reaction, *RSC Adv.*, 2019, **9**(58), 33814–33822.

62 X. Liu, Y. Bu, T. Cheng, W. Gao and Q. Jiang, Flower-like carbon supported Pd–Ni bimetal nanoparticles catalyst for formic acid electrooxidation, *Electrochim. Acta*, 2019, **324**, 134816.

63 S. Ghosh and C. R. Raj, Pt–Pd nanoelectrocatalyst of ultralow Pt content for the oxidation of formic acid: towards tuning the reaction pathway, *Chem. Sci. J.*, 2015, **127**(5), 949–957.

64 Y. M. Asal, A. M. Mohammad, S. S. Abd El Rehim and I. M. Al-Akraa, Synergistic enhancement of formic acid electro-oxidation on Pt_xCu_y co-electrodeposited binary catalysts, *J. Saudi Chem. Soc.*, 2022, **26**(2), 101437.

65 Z. Zhang, Y. Gong, D. Wu, Z. Li, Q. Li, L. Zheng, W. Chen, W. Yuan and L. Y. Zhang, Facile fabrication of stable PdCu clusters uniformly decorated on graphene as an efficient

electrocatalyst for formic acid oxidation, *Int. J. Hydrogen Energy*, 2019, **44**(5), 2731–2740.

66 B. Chang, Z. Ai, D. Shi, Y. Zhong, K. Zhang, Y. Shao, L. Zhang, J. Shen, Y. Wu and X. Hao, p–n tungsten oxide homojunctions for vis-NIR light-enhanced electrocatalytic hydrogen evolution, *J. Mater. Chem. A*, 2019, **7**(33), 19573–19580.

67 Y. Zhou, Y. Yang, X. Zhu, T. Zhang, D. d. Ye, R. Chen and Q. Liao, Novel Superaerophobic Anode with Fern-Shaped Pd Nanoarray for High-Performance Direct Formic Acid Fuel Cell, *Adv. Funct. Mater.*, 2022, 2201872.

68 M. Hosseini and M. Momeni, Evaluation of the Performance of Platinum Nanoparticle–Titanium Oxide Nanotubes as a New Refreshable Electrode for Formic Acid Electro-oxidation, *Fuel Cells*, 2012, **12**(3), 406–414.

69 S. R. Chowdhury and T. Maiyalagan, Enhanced electrocatalytic activity of nitrogen-doped reduced graphene oxide supported PdCu nanoparticles for formic acid electrooxidation, *Int. J. Hydrogen Energy*, 2019, **44**(29), 14808–14819.

70 L. Ye, A. H. Mahadi, C. Saengruengrit, J. Qu, F. Xu, S. M. Fairclough, N. Young, P.-L. Ho, J. Shan and L. Nguyen, Ceria nanocrystals supporting Pd for formic acid electrocatalytic oxidation: prominent polar surface metal support interactions, *ACS Catal.*, 2019, **9**(6), 5171–5177.

71 D. Bin, B. Yang, F. Ren, K. Zhang, P. Yang and Y. Du, Facile synthesis of PdNi nanowire networks supported on reduced graphene oxide with enhanced catalytic performance for formic acid oxidation, *J. Mater. Chem. A*, 2015, **3**(26), 14001–14006.

72 H. Lu, Y. Fan, P. Huang and D. Xu, SnO_2 nanospheres supported Pd catalyst with enhanced performance for formic acid oxidation, *J. Power Sources*, 2012, **215**, 48–52.

73 Z. Yuan, T. Cao, M. Deng, J. Ma, S. Geng, C. Yang., Y. Ren, M. Yao, F. Liu and X. Wang, Unveiling the CeO_2 morphology effect in Pd-CeO_2/C heterostructures catalysts for formic acid dehydrogenation, *Fuel*, 2023, **346**, 128333.